Supporting Information

A Harsh-Environment Tolerant, Ultra-strong yet Tough Bio-Based Adhesive via General Branched-Topology Engineering: Break Adhesion–Toughness Conflicts

Qikai Zhu,[+a] *Lifen Yang,*[+b] *Yang Zhang,*[a] *Jiayi Yang,*[a] *Jingyi Rao**[c], *Zhuanggui Chen**[b], *and Dingshan Yu**[a]

[a] Key Laboratory for Polymeric Composite and Functional Materials of Ministry of Education, Key Laboratory of High Performance Polymer-based Composites of Guangdong Province, GBRCE for Functional Molecular Engineering, School of Chemistry, Sun Yat-sen University Guangzhou, 510006, China. E-mail: yudings@mail.sysu.edu.cn.

[b] Department of Children's Medical Center and department of Allergy, The Third Affiliated Hospital of Sun Yat-sen University, Guangzhou Key Laboratory of Research and Innovation Technology Translation for Airway Inflammatory Diseases, Sun Yat-sen University Guangzhou, 510006, China. E-mail: chzhgui@mail.sysu.edu.cn.

[c] State Key Laboratory of Materials Processing and Die & Mould Technology, and Hubei Key Laboratory of Bioinorganic Chemistry and Materia Medica, School of Chemistry and Chemical Engineering, Huazhong University of Science and Technology, Wuhan 430074, P. R. China. E-mail: jrao@hust.edu.cn.

[*]Corresponding author. Correspondence and requests for materials should be addressed to: yudings@mail.sysu.edu.cn.

Experimental Section

1. Materials

All chemicals and solvents were purchased from commercial sources and used as received without further purification. (E)-5-(4-Hydroxystyryl)benzene-1,3-diol (resveratrol) were acquired from Shanghai Bide Pharmatech Co., Ltd. Ethylene glycol diglycidyl ether (EGDE), 1,4-Butanediol diglycidyl ether (BDDE), 1,6-Hexanediol Diglycidyl Ether (HDDGE), potassium hydroxide (KOH), sodium chloride (NaCl), tetrahydrofuran (THF), *N*,*N*-Dimethylformamide (DMF), anhydrous ethanol (EtOH), petroleum ether (PE) and ethyl acetate (EA) were purchased from Shanghai Macklin Biochemical Co., Ltd. Concentrated hydrochloric acid (HCl) was purchased from Guangzhou Chemical Reagent Factory.

2. Characterization instruments and methods

The attenuated total reflection-Fourier transform infrared (ATR-FTIR) spectra were recorded using a Thermo Nicolet iS50 spectrometer. Tensile strength, toughness, and lap shear strength data were obtained using a universal electronic tensile testing machine (Instron 5969, Instron Co., Ltd., United States) equipped with a 2 kN load cell. The glass transition temperatures (T_g) were determined by differential scanning calorimetry (DSC, NETZSCH DSC 214). Thermal decomposition behavior was evaluated from thermogravimetric analysis (TGA, NETZSCH TG 209F1 Libra). The morphology and microstructure of the samples were characterized using a scanning electron microscope (SEM, Hitachi S-4800, Japan) equipped with a cold field emission gun, operated at an accelerating voltage of 10.0 kV. The molecular weight and molecular weight distribution of the polymer were characterized using a Waters 1515 gel permeation chromatograph (GPC). Small-angle X-ray scattering (SAXS) spectra were acquired using the Xuess2.0 system (Xenocs, France). The positron lifetime spectrum was acquired using a positron annihilation lifetime spectrometer (Model: ORTEC PLS2-SYSTEM). The water contact angle measurements of the samples were conducted using an OCA50 automatic video optical contact angle meter (DataPhysics, Germany). Atomic force microscopy

(AFM) measurements of the samples were conducted using a Bruker Multimode 8 system operating in PeakForce Quantitative Nanomechanics (QNM) mode. Dynamic mechanical analysis (DMA) measurements of the samples were performed using a TA Instruments DMA 8500 dynamic mechanical analyzer. Strain-responsive electrical signals were acquired using a flexible sensor acquisition card (Dalian, China).

3. Experimental details

3.1. Preparation adhesives and lap shear test

3.1.1. Preparation of precursor adhesives for adhesion. To fabricate bio-based epoxy adhesives (BSFA), a facile one-pot synthesis approach was employed: under triethylamine catalysis, resveratrol was separately reacted with an excess of di-glycidyl ethers with varied flexible chain lengths—including ethylene glycol diglycidyl ether (EGDE), 1,4-butanediol diglycidyl ether (BDDE), and 1,6-hexanediol diglycidyl ether (HDDGE)—at a molar ratio of 1:2 and 65 °C for 3 hours, yielding three one-component prepolymers.

3.1.2. Lap shear test. The lap shear test was conducted in accordance with a modified version of ASTM F2255-05 (2005) at a constant tensile rate of 4 mm min^{-1}. The maximum tensile force (F_{max}) was recorded, and the adhesive strength (MPa) was calculated by dividing F_{max} by the bonding area. At least five replicate measurements were performed for each sample to determine mean values and error bars.

$$\text{L}ap\ shear\ strength = \frac{F_{max}}{\text{Adhesive}\ area} \quad (1)$$

3.1.3. Testing of adhesives for resistance to various temperatures. Two stainless steel plates were bonded with the aforementioned adhesive to yield test specimens. For extreme low-temperature testing: the adhesive was exposed to liquid nitrogen (-196 °C) for 24 hours, followed by immediate assessment of its load-bearing capacity for a 22 kg weight within 30 seconds to observe if it failed. For low- and high-temperature testing: the specimens were

placed in a universal testing machine equipped with a temperature-controlled chamber, where six temperatures (-20 °C, 0 °C, 25 °C, 50 °C, 80 °C, and 120 °C) were set sequentially, with each temperature held for 10 minutes. Subsequent to temperature exposure, the specimens were promptly subjected to tensile testing within 30 seconds. Five parallel specimens were utilized for each measurement.

3.1.4. Testing of BSFA adhesives for resistance to various harsh conditions. BSFA2 and BSFA3 adhesives were utilized to bond stainless steel, phenolic bakelite (PF), and wood substrates. The resulting bonded assemblies were subsequently immersed in hot water (63 °C) and boiling water (100 °C) for 3 hours. Additionally, epoxy glass fiber–reinforced plastic (EP) and phenolic bakelite (PF) specimens joined with BSFA2 and BSFA3were exposed to a 10 wt% aqueous NaCl solution (pH 7), an acidic medium (1 mol/L), and an alkaline medium (1 mol/L) for 1 day. BSFA2/BSFA3-bonded steel plates were similarly immersed in deionized water and four common organic solvents—petroleum ether, 95% anhydrous ethanol, ethyl acetate, and tetrahydrofuran—for 7 days. Following immersion, the adhesive joints were subjected to tensile testing under wet conditions. All measurements were performed using five parallel specimens to ensure statistical reliability.

3.2. Thermogravimetric Analysis (TGA)

Thermogravimetric analysis (TGA) was carried out using a NETZSCH TG 209F1 Libra thermogravimetric analyzer under a nitrogen atmosphere at a heating rate of 20 °C min^{-1} over a temperature range from 30 °C to 800 °C.

3.3. Scanning electron microscopy (SEM)

3.3.1. Preparation of sample surfaces for SEM measurements. The surfaces of stainless steel substrates separated after lap shear test were sprayed with gold and the microstructural morphology was observed using cold field emission SEM at an accelerating voltage of 10 kV.

3.3.2. Preparation of sample fracture surfaces for SEM measurements. The cured films

were fractured in liquid nitrogen and another one is fractured after tensile test and then coated with gold, and the fracture cross-sectional morphology was observed using cold field emission SEM at an accelerating voltage of 10 kV.

3.4. Differential scanning calorimeter (DSC)

Differential scanning calorimetry (DSC) measurements were conducted using a NETZSCH DSC 214 instrument. Samples weighing 3–5 mg were analyzed under a nitrogen atmosphere at a heating and cooling rate of 20 °C min^{-1} over a temperature range from −70 °C to 160 °C. Data were recorded during the second heating cycle.

3.5. Small Angle X-ray Scattering test (SAXS)

Small-angle X-ray scattering (SAXS) measurements were carried out using a Xeuss 2.0 system (Xenocs, France) equipped with an incident X-ray wavelength of 0.154 nm. Two-dimensional SAXS patterns were collected with a Pilatus 200K detector at a fixed sample-to-detector distance of 1670 mm and an exposure time of 20 min.

3.6. Gel Permeation Chromatography (GPC) Analysis

The molecular weight and its distribution of the polymer were characterized using a Waters 1515 gel permeation chromatograph (GPC) equipped with a 2414 differential refractive index (RI) detector. HPLC-grade N,N-dimethylformamide (DMF) containing 0.1 mol/L lithium bromide (LiBr) was employed as the mobile phase. Separation was achieved on a series of Styragel HR columns at a constant flow rate of 1.0 mL/min, with both the column oven and detector temperatures maintained at 40 °C. Samples were prepared at a concentration of 2–3 mg/mL, filtered through a 0.45 μm membrane filter prior to injection, and universal calibration was performed using narrow-dispersion poly(methyl methacrylate) (PMMA) standards.

3.7. Tensile tests

Tensile tests were performed using a universal electronic tensile testing machine (Instron 5969, Instron Co., Ltd., United States) with a 2 kN load cell at room temperature. The BSFA adhesive prepolymer was poured into a polytetrafluoroethylene (PTFE) mold, followed by curing at 120 °C for 3 hours in a vacuum oven to yield dumbbell-shaped test specimens with dimensions of 40 mm × 2.0 mm × 1.0 mm, which were tested at a stretching rate of 4 mm min^{-1}. Ture stress (σ_t) and ture strain (ε_t) were calculated based on the engineering stress-strain curve by the following equation 1 and 2, respectively.

$$\sigma_t = \sigma * \frac{L}{L_0} \sigma\ (1 + \varepsilon) \tag{2}$$

$$\varepsilon_t = \int_{L_0}^{L} \frac{dL}{L} = ln \frac{L}{L_0} = ln\ (1 + \varepsilon) \tag{3}$$

where σ is the tensile strength, L is the instant length of the deformed sample, L_0 is the original length of the sample, and ε is the elongation at break.

Tensile toughness of the samples was calculated as the area under the engineering stress-strain curve, obtained at a stretching speed of 4 mm min^{-1}, according to the following equation:

$$Toughness = \int_{\varepsilon=0}^{\varepsilon=\varepsilon_{max}} \sigma\, d\varepsilon \tag{4}$$

where σ is the tensile strength, ε is the elongation at break, and ε_{max} is the elongation at break of the sample.

Stepwise cyclic tensile tests were conducted at a strain rate of 4 mm min^{-1} and a recovery rate of 4 mm min^{-1} at room temperature. BSFA3 was subjected to incrementally increasing strain levels ranging from 25% to 200% without holding time between cycles. The energy dissipation was determined by integrating the area enclosed by the stress–strain hysteresis loop.

3.8. Positron annihilation lifetime spectroscopy (PALS) measurement

PALS is based on the principle that positron and positronium lifetimes are sensitive to structural inhomogeneities, as the formation and annihilation of positronium (Ps)—the bound state of a positron (e^+) and an electron (e^-)—occur preferentially within nanoscale or

subnanoscale holes.[1]

Each lifetime spectrum was deconvoluted into three distinct lifetime components using the LTv9 software. The short-lived component (τ_1) and the intermediate-lived component (τ_2) are associated with para-positron (*p*-Ps) annihilation, while the longest-lived component (τ_3) corresponds to the pick-off annihilation of ortho-positronium (*o*-Ps). The lifetime and intensity of o-Ps are directly related to the size and concentration of free-volume holes in the polymer matrix. Using the Tao-Eldrup model,[2] the average radius (R) of the free-volume holes can be estimated from the *o*-Ps lifetime τ_3.

$$\tau_3^{-1} = 2[1 - \frac{R}{R+\Delta R} + \frac{1}{2\pi}\sin(2\pi\frac{R}{R+\Delta R})] \quad (5)$$

Where ΔR corresponds to the thickness of the electron layer on the surface of the free-volume holes, which is an empirical value (0.1656 nm) for polymers. The average size of free-volume holes (v_f) can be calculated:

$$V_f = \frac{4\pi R^3}{3} \quad (6)$$

The relative fraction free volume (*FFV*) f_r (%) is defined as:

$$f_r = V_f I_3 \quad (7)$$

Where I_3 is *o*-Ps intensity.

3.9. Water contact angle measurement

Water contact angle measurements of the samples were performed using an OCA50 automatic video optical contact angle meter from Dataphysics (Germany). A 3 μL water droplet was dispensed, and the contact angle values were calculated by fitting the droplet profile with the Young-Laplace equation. Each sample was measured at least five times, and the average

value was reported. Prior to characterization, the BSFA adhesive prepolymer was cast into a polytetrafluoroethylene (PTFE) mold and cured at 120 °C in a vacuum oven for 3 hours to prepare the test film samples.

3.10. Atomic force microscopy (AFM) measurements

Atomic force microscopy (AFM) measurements were carried out using a Bruker Multimode 8 system operated in peak force tapping mode with quantitative nanomechanical mapping (QNM). The tests were performed at room temperature (25 °C) with a scanning frequency of 1 Hz. Prior to characterization, the BSFA adhesive prepolymer was cast into a polytetrafluoroethylene (PTFE) mold and cured in a vacuum oven at 120 °C for 3 hours to prepare the thin film samples.

3.11. Dynamic Mechanical Analysis (DMA)

The DMA8500 model dynamic mechanical analyzer produced by TA Company was used for the test. The test mode was tensile mode, with a frequency of 1 Hz and a heating and cooling rate of 3 °C/min. The temperature scanning range was -60 to 50 °C, and the amplitude was 1%. The sample was first cooled to -60 °C, then held for 5 minutes before being heated to 50 °C. The changes in modulus and loss factor during the entire heating process were recorded.

3.12. Antibacterial adhesion test

First, the liquid Luria-Bertani broth (LB) medium was subjected to ultraviolet sterilization. The cured BSFA3 adhesive was sectioned into discs with a diameter of 6 mm and then placed in a 96-well cell culture plate. Subsequently, 1 mL of the bacterial suspension was added, and the plate was incubated at 37 °C for 24 hours. The culture medium was carefully aspirated, and the samples were rinsed three times with sterile phosphate-buffered saline (PBS). Bacterial cells were then fixed with 2.5% glutaraldehyde solution for 30 min at room temperature.

Subsequently, the samples were dehydrated through a graded ethanol series (20%, 50%, and 70% v/v) and processed for scanning electron microscopy (SEM) observation.

3.13. The strain response electrical signals and gauge factor tests

The strain response electrical signals were conducted by the Flexible sensor acquisition card (Dalian, China), the calculation equation for the relative resistance change ($\Delta R/R_0$) was as follows:

$$\frac{\Delta R}{R_0} = \frac{R - R_0}{R_0} \times 100\% \quad (8)$$

where R_0 and R are the initial and strained resistances, respectively.

Supplementary Figures

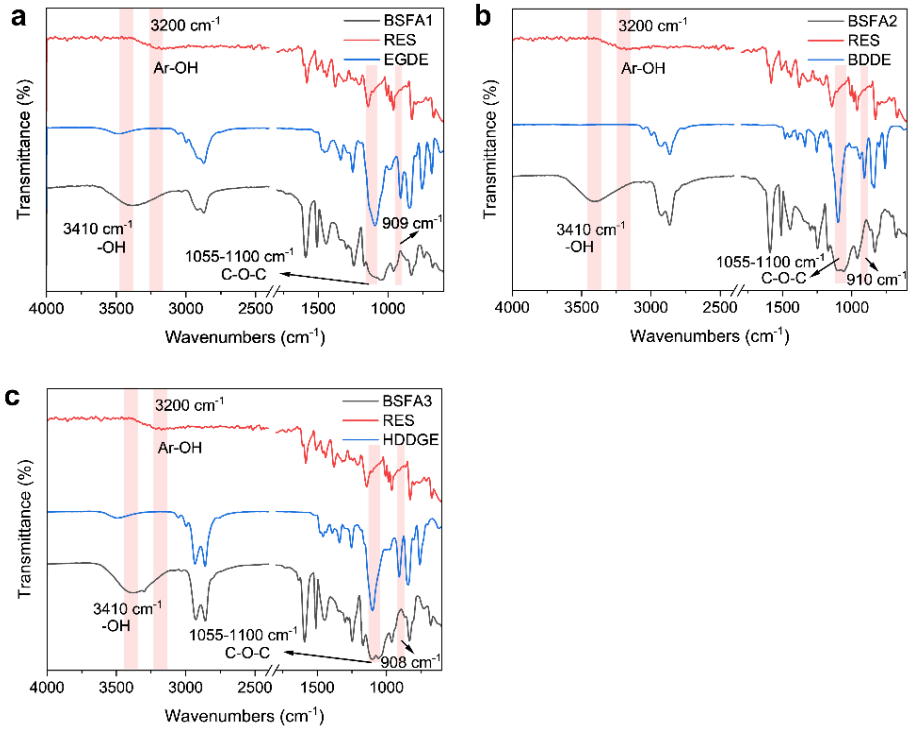

Figure S1. ATR-FTIR spectra of a) BSFA1, b) BSFA2, c) BSFA3. The epoxy group is observed at the wavenumber of 910 cm^{-1}.

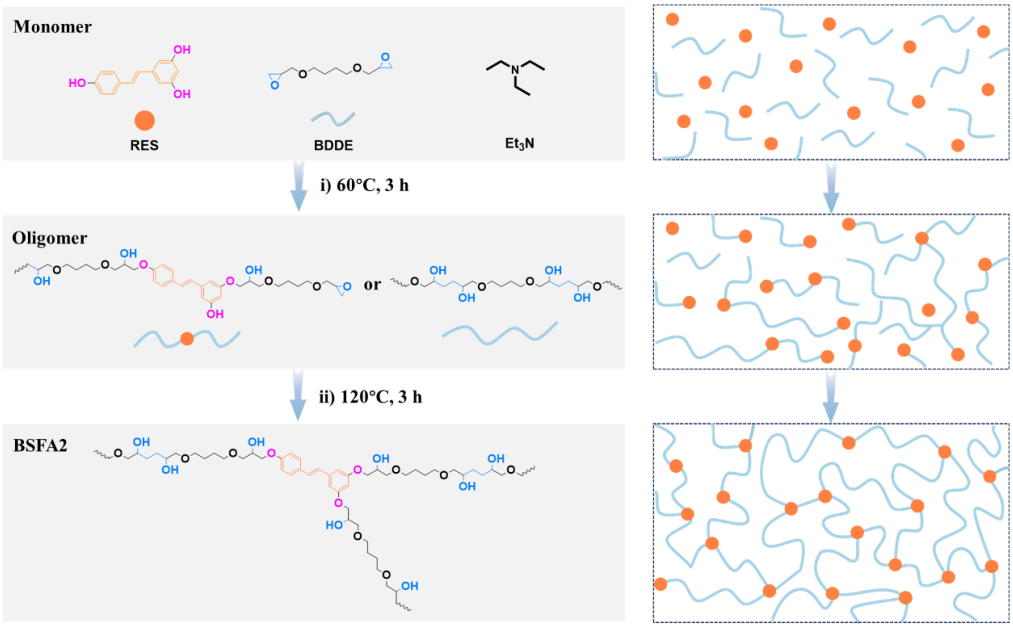

Figure S2. Schematic Illustration of the Synthesis and Curing Pathways for the BSFA Series

(Exemplified by BSFA2).

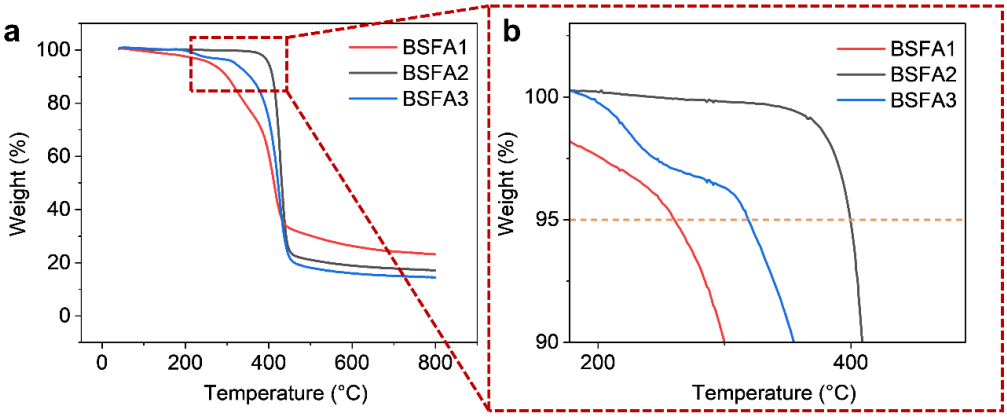

Figure S3. TG analysis. a) TG curve of BSFA and b) its local enlarged image.

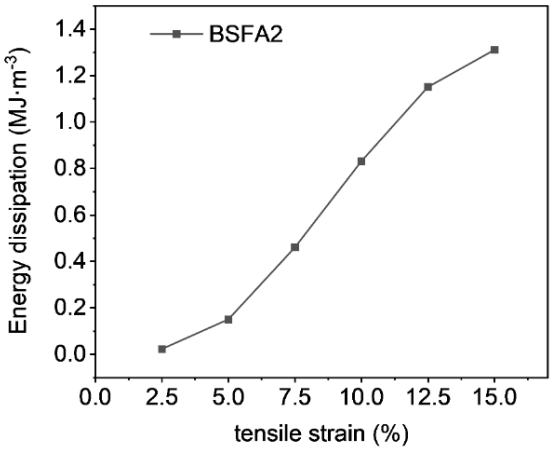

Figure S4. The energy dissipation of BSFA2 with increasing strain from 2.5 to 15.0%

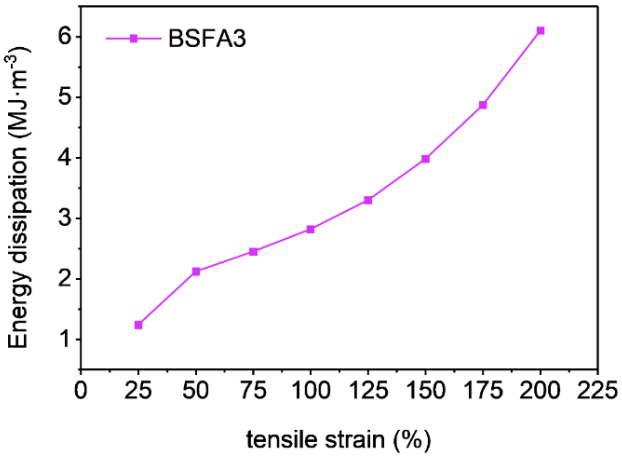

Figure S5. The energy dissipation of BSFA3 with increasing strain from 25 to 200%

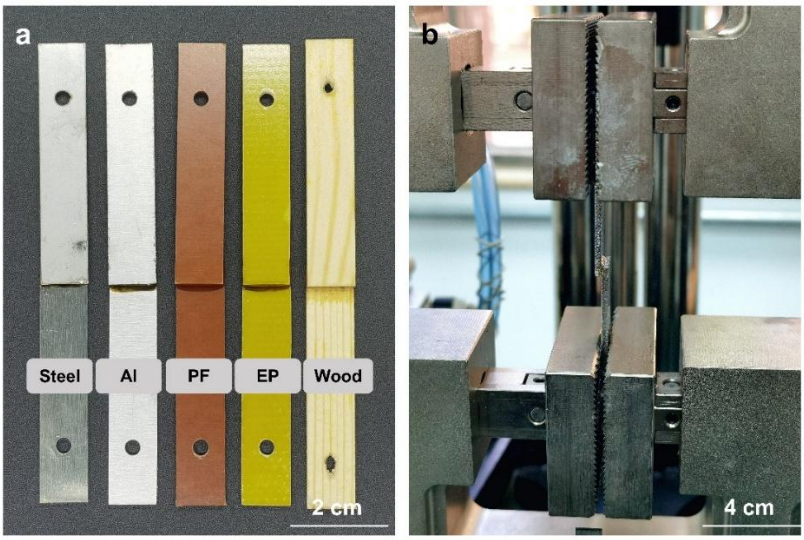

Figure S6. a) Photograph of various sheets bonded with BSFA2. b) Photograph of lap shear test.

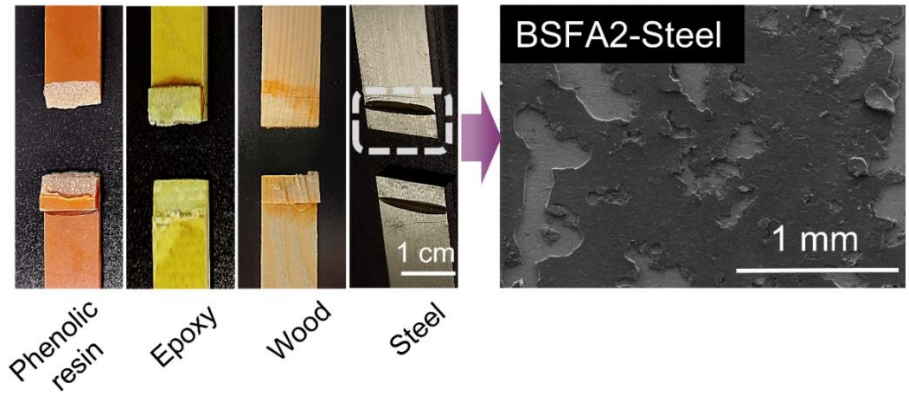

Figure S7. Images of adhesive failure of BSFA2 bonded to different substrates after lap shear testing, along with SEM images of its adhesive failure on stainless steel substrates.

Figure S8. A schematic diagram of BSFA3 adhered to a stainless steel substrate and immersed in liquid nitrogen (-196 °C) for 24 hours, then lifting a 22-kilogram kettlebell.

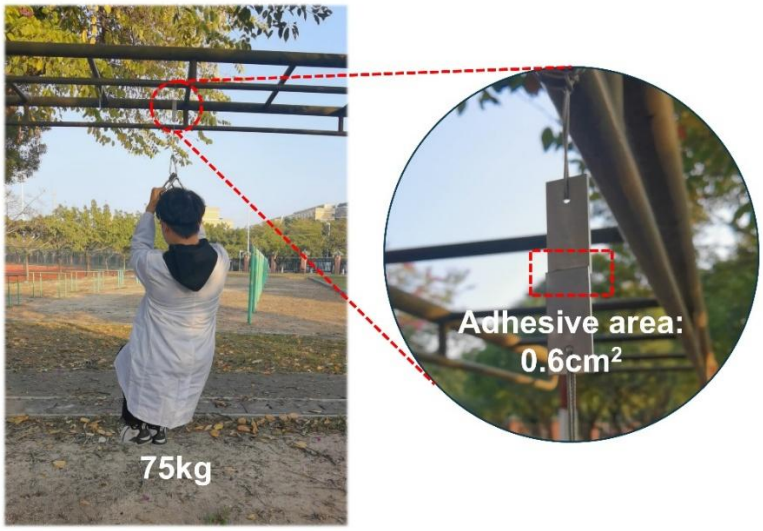

Figure S9. Optical Image Demonstrating that BSFA2 with a Bonding Area of Merely 0.6 cm^2 Can Easily Support a 75-kg Adult Male.

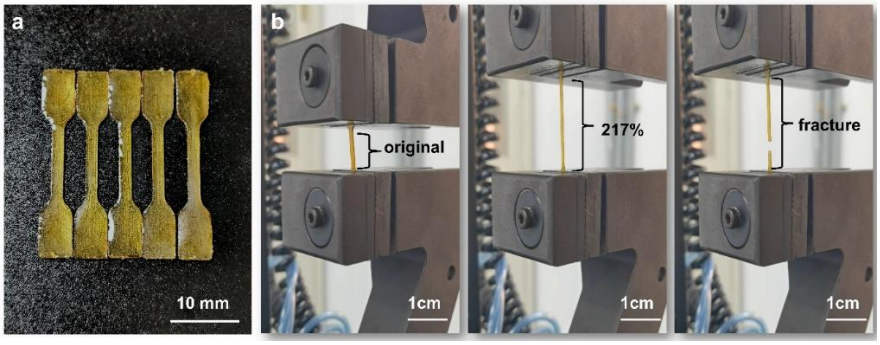

Figure S10. Optical images of BSFA3 during tensile testing. a) Dumbbell-shaped specimens fabricated via polytetrafluoroethylene (PTFE) molds. b) Fracture image from BSFA3 tensile test.

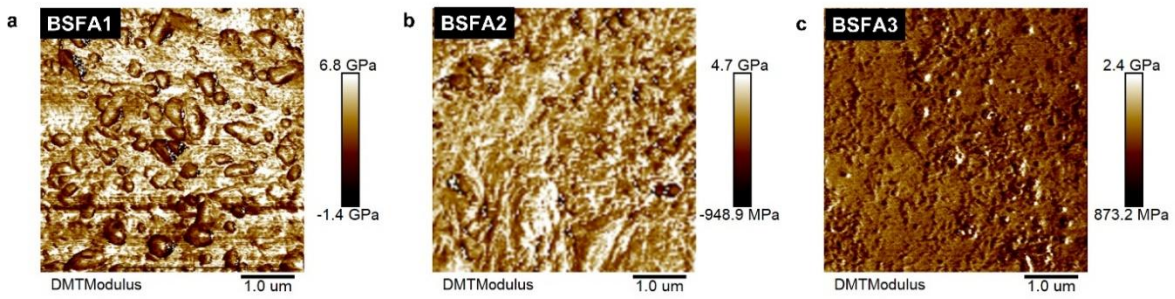

Figure S11. Distribution of Young's modulus measured by AFM. a) BSFA1, b) BSFA2, c) BSFA3.

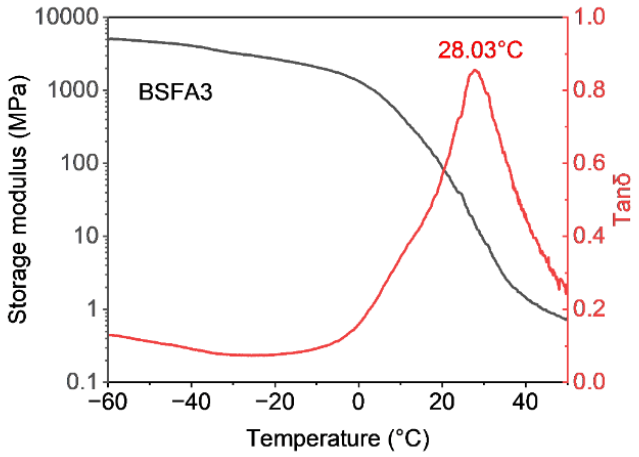

Figure S12. Dynamic thermo-mechanical properties. Storage modulus and loss factor of BSFA3 as a function of temperature.

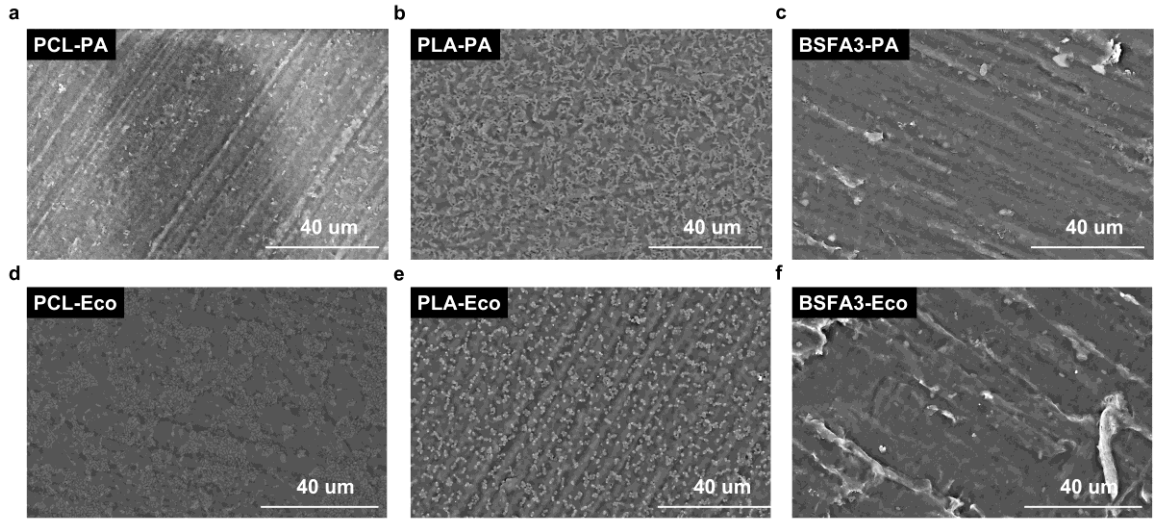

Figure S13. Scanning electron microscopy (SEM) images of antibacterial adhesion behavior of BSFA3, commercial polycaprolactone (PCL), and polylactic acid (PLA) films. Among them, PA refers to Pseudomonas aeruginosa and Eco refers to Escherichia coli.

The above results demonstrate that BSFA3 exhibits excellent anti-adhesion activity against bacteria and can effectively suppress bacterial aggregation on the material surface. Its antibacterial performance may be attributed to two key factors: (1) the inherent phenolic hydroxyl groups of resveratrol, which disrupt bacterial cell membranes;[3,4] and (2) the moderate hydrophobicity of the BSFA3 system, as evidenced by a water contact angle of 93.34°, which hinders bacterial adhesion to the surface.

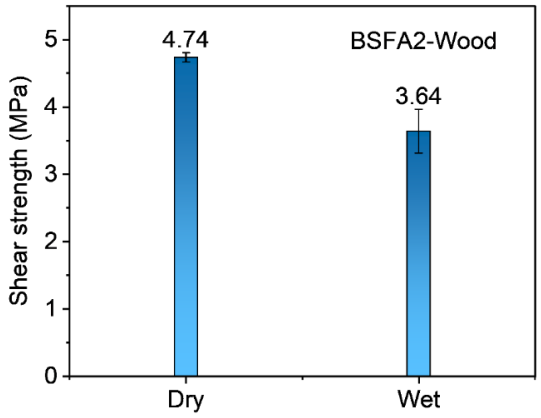

Figure S14. Dry and wet shear strengths of three-layer laminates bonded with BSFA2. The

"wet" condition refers to soaking in 63°C hot water for 3 hours.

Figure S15. The wet shear strength of three-layer laminates bonded with BSFA2 was evaluated through lap shear testing. Fracture surface analysis after testing revealed substrate failure (pine wood), indicating that the actual bonding strength exceeds the measured value.

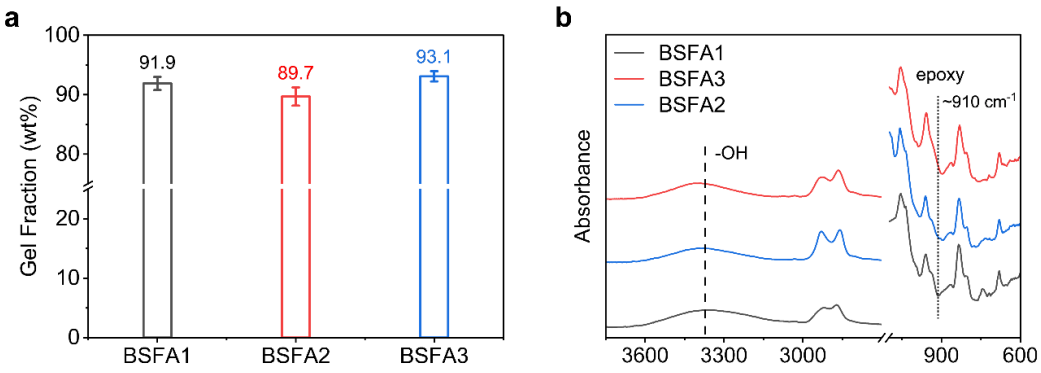

Figure S16. Validation of curing degree for the BSFA system. a) Gel fractions of the cured BSFA networks: error bars denote the standard deviation from three parallel specimens. b) FT-IR spectra of cured BSFA.

Gel Fraction Determination: polymer films were embrittled in liquid nitrogen for 10 min and

ground into powder using a cryogenic mill. A portion of the powder was wrapped in pre-weighed dry filter paper and weighed (M_1)). The wrapped sample was refluxed with analytical-grade acetone in a Soxhlet extractor for 48 h. After extraction, the package was dried at 80 °C under vacuum until constant weight, cooled, and reweighed (M_3). (M_2) is the mass of the empty filter paper. Each sample was tested in triplicate. Gel fraction was calculated using the relevant formula.

$$\text{Gel content (wt\%)} = \frac{(M_3 - M_2)}{(M_1 - M_2)} \times 100\% \quad (9)$$

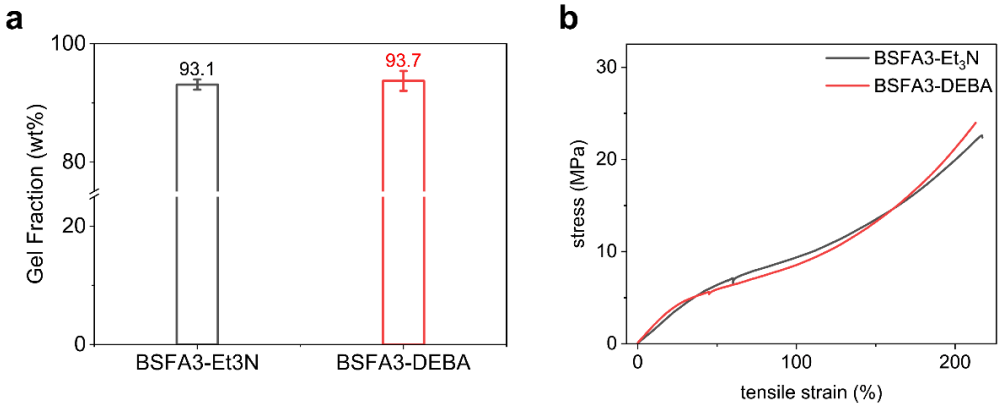

Figure S17. Performance Comparison of BSFA3 Cured with Different Catalysts. a) Gel fractions of BSFA3 networks cured with different catalysts: error bars represent the standard deviation of three parallel samples.

To mitigate environmental pollution risks associated with catalyst volatilization and address the scalability requirements of industrial manufacturing, the feasibility of substituting triethylamine with high-boiling-point catalysts was further investigated, as detailed below:

BSFA3 samples were fabricated using *N*,*N*-dimethylbenzylamine (DEBA; boiling point: 183–184 °C) as a replacement for triethylamine. Both catalysts were dosed at 1 wt% under identical reaction and curing conditions. Comparative analysis revealed that the gel fractions of DEBA-catalyzed samples (93.7%) were comparable to those of triethylamine-catalyzed counterparts (93.1%), with no significant difference in the mechanical properties of the resultant specimens.

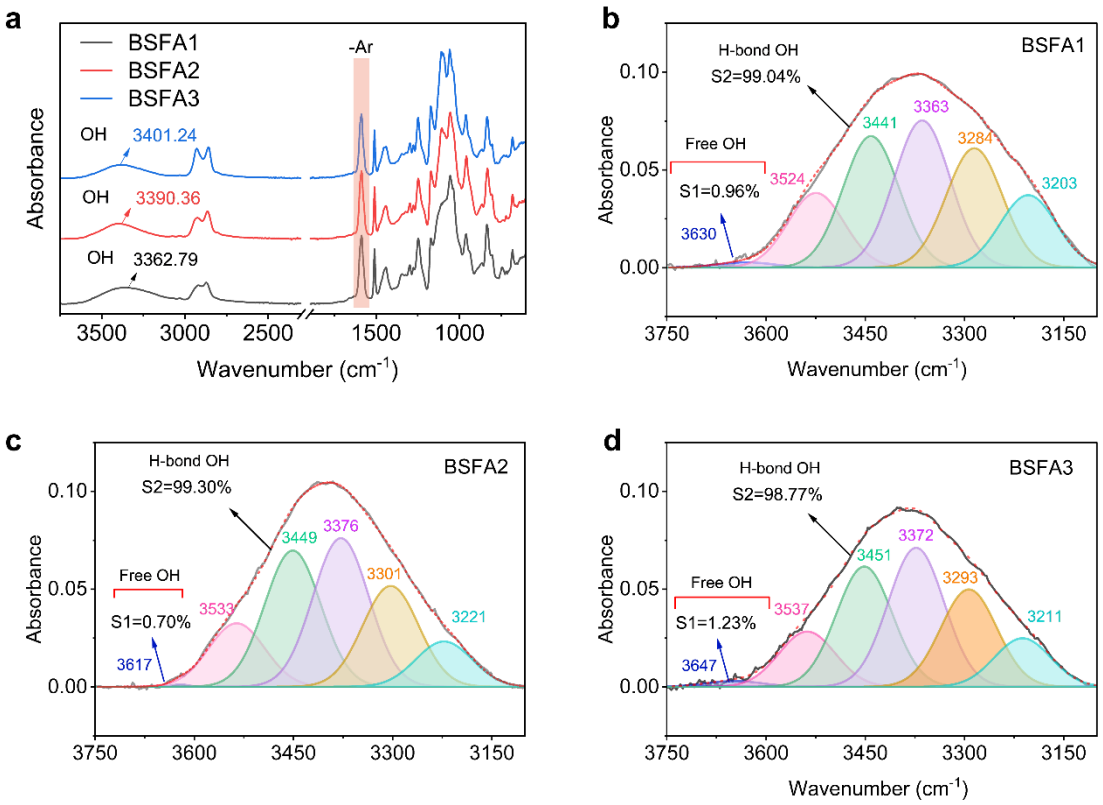

Figure S18. a) Attenuated total reflection fourier transform infrared (ATR-FTIR) spectra of cured BSFA series samples**.** b-d) O–H stretching vibration peak of cured BSFA samples.

Specifically, to minimize moisture interference with the infrared hydroxyl peak of BSFA-based films, all cured polymers were uniformly dried in an 80 °C vacuum oven for 48 h, followed by static cooling in the same oven. Spectroscopic measurements were immediately performed using attenuated total reflection Fourier-transform infrared (ATR-FTIR) spectroscopy. Given the identical raw material ratios across different BSFA systems and the chemical inertness of resveratrol's benzene ring throughout the reaction and curing processes, the characteristic benzene ring peak (~1600 cm^{-1}) was employed as an internal standard to enable reliable comparison of the relative concentration of hydroxyl groups among BSFA systems with varying flexible chain lengths—this approach eliminates potential errors arising from differences in the thickness of cured films. For each system, the hydroxyl peak and benzene ring peak were integrated separately, and the ratio of the hydroxyl peak area to the internal standard benzene ring peak area was used to quantify the relative concentration of hydroxyl groups.

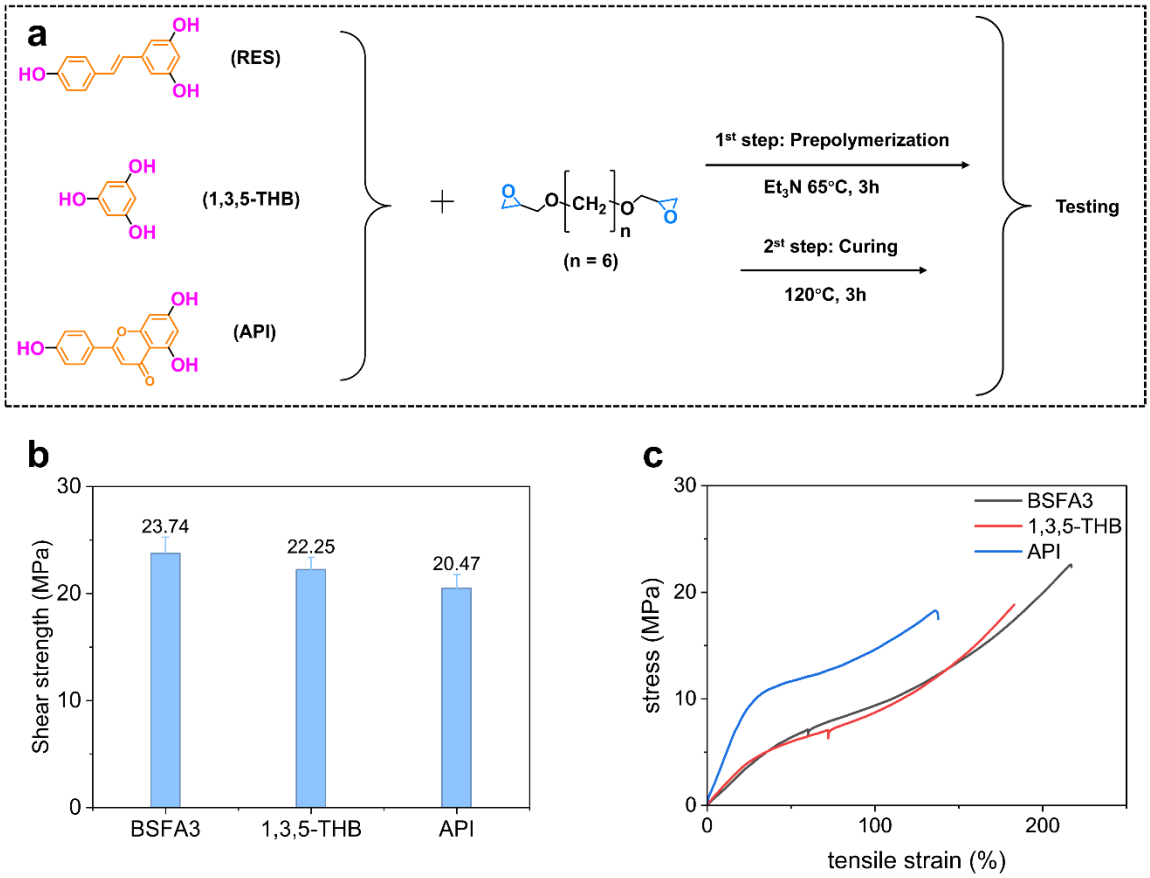

Figure S19. Validation of the Method's Universality. a) Schematic illustration of the reaction routes between three monomers—resveratrol (RES), 1,3,5-trihydroxybenzene (1,3,5-THB), and apigenin (API)—and HDE. b) Comparison of bonding performance among the above rigid core-based systems. c) Comparison of mechanical properties among the above rigid core-based systems.

To verify the universality of the proposed method, different rigid triphenol cores were reacted with 1,6-hexanediol diglycidyl ether (HDE), and the bonding strength and mechanical properties of the resulting materials were characterized. The above results demonstrate that the preparation method employed in this study exhibits excellent universality, which can be readily extended to other rigid monomers with analogous structures, enabling the fabrication of a series of robust and tough adhesives.

Supplementary Tables

Table S1. Gel Permeation Chromatography (GPC) Characterization Results of the BSFA Series Prepolymers.

Samples	M_n	M_w	M_z	M_{z+1}	Polydispersity
BSFA1	2562	2564	2567	2569	1.000860
BSFA2	2526	2527	2528	2529	1.000338
BSFA3	2571	2574	2576	2579	1.000962

Table S2. Thermal properties of BSFA.

Samples	T_g (°C)	$T_{d,5\%}$ (°C)	Residual mass fraction (%)
BSFA1	95.28	260.39	23.16
BSFA2	65.16	399.13	17.16
BSFA3	32.13	318.65	14.47

Table S3. Mechanical properties of BSFA.

Samples	Tensile strength (MPa)	Tensile modulus (MPa)	Elongation at break (%)	Toughness ($MJ \cdot m^{-3}$)
BSFA1	48.43	1220.00	6.33	2.00
BSFA2	33.41	738.20	15.29	4.01
BSFA3	22.37	21.49	217.20	23.27

Table S4. Peak region of the O–H infrared stretching vibration band for BSFA.

Samples	BSFA1		BSFA2		BSFA3	
	Peak position	Peak area (%)	Peak position	Peak area (%)	Peak position	Peak area (%)
free OH(S1)	3630.34	0.96	3617.64	0.70	3647.43	1.23
hydrogen bond OH(S2)	3524.22	13.57	3533.22	13.18	3537.62	11.86
	3441.06	23.92	3449.01	27.71	3451.10	25.81
	3363.61	26.77	3376.23	29.59	3372.75	29.83
	3284.77	21.71	3301.19	19.90	3293.04	20.90
	3203.20	13.07	3221.14	8.92	3211.74	10.38
total		100		100		100

Table S5. Integral results of O–H and benzene ring vibrations, and infrared semi-quantitative calculation outcomes for BSFA.

Samples	Peak integral area (-OH)	Peak integral area (-Ar, 1540–1660 cm^{-1})	Ratio (-OH/Ar, All OH)	Proportion (H-bonds OH)
BSFA1	23.35	63.09	2.70	2.68
BSFA2	23.5	60.12	2.56	2.54
BSFA3	20.22	48.69	2.41	2.38

Table S6. Bio-based carbon content (%) of different cured BSFA adhesives.

Samples	BSFA1	BSFA2	BSFA3
Carbon content (%)	44.8	41.2	36.8

The carbon content of the BSFA series of bio-based materials is estimated in accordance with the EN 16785-2 standard issued by the European Committee for Standardization (CEN). Calculate the bio-based carbon content, as a percentage of the total mass of the sample,

$$\boldsymbol{X_B} = \frac{\sum_i^n \boldsymbol{W_i} \cdot \boldsymbol{X_{B,i}}}{\boldsymbol{W}} \quad (10)$$

where

$\boldsymbol{n}$ is the number of constituents of the sample;

$\boldsymbol{W}$ is the total mass of the sample;

$\boldsymbol{W_i}$ is the mass of the constituent *i*;

$\boldsymbol{X_B}$ is the bio-based carbon content, expressed as a percentage of the total mass of the sample;

$\boldsymbol{X_{B,i}}$ is the bio-based carbon content of the constituent i, expressed as a percentage of the mass of the constituent *i*.

Table S7 Comparison of the mechanical properties of the proposed material (BSFA3) with those of toughened epoxy resins from the literature.

Reference	Toughening mechanism	tensile strength (MPa)	Elongation at break (%)	Toughness ($MJ \cdot m^{-3}$)
This work - BSFA3	Homogeneous Toughening via Flexible Chains	22.37	217.20	23.27
1	Hyperbranched topological structure[5]	104.50	5.65	3.58
2	H-bonds[6]	14.70	184.00	7.50
3	Network topology[7]	48.00	9.70	4.70
4	Sacrificial reversible ironcatechol cross-links[8]	21.90	172.00	22.00
5	Rubber filler[9]	39.00	11.00	5.90
6	Hyperbranched structure[10]	114.43	3.57	2.15
7	Block copolymer[11]	63.70	8.00	3.50
8	Rubber filler[12]	76.70	11.30	4.30
9	Inorganic filler[13]	72.00	4.80	1.80
10	Inorganic filler[14]	97.10	4.40	2.50
11	Network topology[15]	51.30	17.90	6.70
12	Network topology[16]	38.90	42.80	14.60
13	Thermoplastics[17]	81.00	2.60	1.70
14	Network topology[18]	40.00	60.00	22.00

Table S8 Comparison of the bonding strength of BSFA2 and BSFA3 with various recently reported bio-based adhesives and synthetic adhesives on stainless steel, wood and aluminum.

	Lap-shear Strength (MPa)		
Reference	**Steel**	**Wood**	**Aluminum**
Bio-based adhesive			
This work - BSFA2	31.52	14.67	15.21
This work - BSFA3	23.74	5.71	8.44
Nature[19]	13.50	6.80	12.70
Science[20]	6.40	4.80	9.50
Science[21]	/	/	10.50
Adv. Mater.[22]	6.03	/	/
Macromolecules[23]	2.00	/	3.00
CCS Chem.[24]	5.42	/	/
ACS nano[25]	/	1.58	/
Green Chem[26]	/	5.71	/
Adv. Funct. Mater.[27]	8.61	3.78	8.79
Adv. Funct. Mater.[28]	3.50	4.20	/
Adv. Funct. Mater.[29]	/	1.02	0.68
Small[30]	3.86	/	/
Synthetic adhesives			
Sci. Adv.[31]	1.60	1.40	/
Nat. Commun.[32]	6.91	8.14	2.79
Nano Letters[33]	/	3.09	5.30
Adv. Funct. Mater.[34]	18.52	6.58	11.43
Small[35]	/	4.60	7.39
Small[36]	6.21	5.66	4.89

Table S9 Comparison of BSFA2 with previously reported strong and tough adhesives.

	Reference	LSS[a] (MPa)	TS[b] (MPa)	LT-Tol[c] (°C)	SS[d] (type)	E-Tol[e] (type)	HT-Tol[f] (°C)	W_d[g] (N/m)
	This Work – BSFA2	31.52	33.41	-196	16	10	120	13628
	This Work – BSFA3	23.74	22.37	-196	16	10	120	11254
1	***Adv. Mater.***[37]	6.97 (Aluminium)	35.86	/	1	/	80	/
2	***ACS Materials Lett.***[38]	10.2	4.54	/	5	/	/	6033
3	***Angew. Chem. Int. Ed.***[39]	10	/	-196	6	10	/	/
4	***Cell Rep. Phys. Sci.***[40]	12.1	23.2	-70	1	9	100	13225
5	***J. Mater. Chem. A.***[41]	12	27.2	-196	9	1	120	12967
6	***Chem. Eng. J.***[42]	10.75	/	/	6	/	/	1541
7	***Adv. Sci.***[43]	14.6	/	-196	11	7	/	5840
8	***Adv. Funct. Mater.***[44]	7.24	1.89	-50	5	/	/	8145
9	***Angew. Chem. Int. Ed.***[45]	6.57	/	-80	2	1	80	/
10	***Sci. Adv.***[31]	1.6	/	-10	5	7	90	35.044

[a]((LSS = Lap shear Strength)); [b]((TS = Tensile Strength)); [c]((LT-Tol = Low temperature tolerance)); [d]((SS = Substrate species)); [e]((E-Tol = Environmental Tolerance)); [f]((HT-Tol = High temperature tolerance)); [g]((W_d = Work of debonding))

Supplementary Movies

Movie S1

Video of steel substrates bonded with BSFA2 (contact area 3 × 20 mm) for lifting a 75 kg adult.

Movie S2

Video of BSFA3-encapsulated circuit boards after 500 hours of immersion in different chemical environments (taking 1 M KOH solution as an example), demonstrating the retention of original functionality.

Supporting References

1 H. J. Zhang, S. Sellaiyan, T. Kakizaki, A. Uedono, Y. Taniguchi, K. Hayashi, *Macromolecules* 2017, **50**, 3933.

2 X. Liu, H. Wu, W. Xu, Y. Jiang, J. Zhang, B. Ye, H. Zhang, S. Chen, M. Miao, D. Zhang, *Adv. Mater.* 2024, **36**, 2308434.

3 T. Zhang, G.-J. E. Nychas, Y. Liu, G. Zhou, Y. Mao, Y. Zhang, P. Dong, X. Yang and L. Zhu, *International Journal of Food Microbiology*, 2026, **451**, 111664.

4 Z. Wang, Y. Wang, H. Wang, H. Gang, N. Zhang, Y. Zhou, S. Gu, Y. Zhuang, W. Xu, G. Ke, Z. Li and H. Yang, *ACS Appl. Mater. Interfaces*, 2023, **15**, 24846–24857.

5 J. Zhang, C. Jiang, G. Deng, M. Luo, B. Ye, H. Zhang, M. Miao, T. Li, D. Zhang, *Nat. Commun.* 2024, **15**, 4869.

6 T. Liu, H. Zhao, D. Zhang, Y. Lou, L. Huang, L. Ma, X. Hao, L. Dong, F. Rosei, W. M. Lau, *Corros. Sci.* 2021, **187**, 109485.

7 M. Sharifi, G. R. Palmese, *J. Mater. Chem. A* 2021, **9**, 1014.

8 E. Filippidi, T. R. Cristiani, C. D. Eisenbach, J. H. Waite, J. N. Israelachvili, B. K. Ahn, M. T. Valentine, *Science* 2017, **358**, 502.

9 X. Yin, Z. Xie, Q. Liu, X. Yuan, X. Hou, J. Zhao, *J. Appl. Polym. Sci.* 2021, **138**, 51248.

10 X. Liu, H. Wu, W. Xu, Y. Jiang, J. Zhang, B. Ye, H. Zhang, S. Chen, M. Miao, D. Zhang, *Adv. Mater.* 2024, **36**, 2308434.

11 J. (Daniel) Liu, Z. J. Thompson, H.-J. Sue, F. S. Bates, M. A. Hillmyer, M. Dettloff, G. Jacob, N. Verghese, H. Pham, *Macromolecules* 2010, **43**, 7238.

12 S. C. Leguizamon, J. Powers, J. Ahn, S. Dickens, S. Lee, B. H. Jones, *Macromolecules* 2021, **54**, 7796.

13 W. Chang, L. R. F. Rose, M. S. Islam, S. Wu, S. Peng, F. Huang, A. J. Kinloch, C. H. Wang, *Compos. Sci. Technol.* 2021, **208**, 108762.

14 S. Zeng, Z. Hou, C. So, H. Wai, D. Jang, W. Lai, L. Sun, Z. Gao, *Polymer* 2022, **256**, 125194.

15 J. Gao, B. A. Patterson, Y. Kashcooli, D. O'Brien, G. R. Palmese, *Compos. Part B Eng.*

2022, **238**, 109857.
16 J. Gao, X. Chu, C. K. Henry, S. C. Santos, G. R. Palmese, *Polymer* 2021, **212**, 123260.
17 H. Chen, Z. Zhu, D. Patil, D. Bajaj, N. Verghese, Z. Jiang, H.-J. Sue, *Polymer* 2023, **270**, 125763.
18 J.-H. Back, C. Hwang, D. Baek, D. Kim, Y. Yu, W. Lee, H.-J. Kim, *Compos. Part B Eng.* 2021, 222, 109058.
19 C. R. Westerman, B. C. McGill, J. J. Wilker, *Nature* 2023, 621, 306.
20 Z. Zhang, E. C. Quinn, J. K. Kenny, A. Grigoropoulos, J. S. DesVeaux, T. Chen, L. Zhou, T. Xu, G. T. Beckham, E. Y.-X. Chen, *Science* 2025, **387**, 297.
21 S. Pal, J. Shin, K. DeFrates, M. Arslan, K. Dale, H. Chen, D. Ramirez, P. B. Messersmith, *Science* 2024, **385**, 877.
22 Y. Wang, E. J. Jeon, J. Lee, H. Hwang, S. Cho, H. Lee, *Adv. Mater.* 2020, **32**, 2002118.
23 C. L. Jenkins, H. M. Siebert, J. J. Wilker, *Macromolecules* 2017, **50**, 561.
24 S. Wu, C. Cai, F. Li, Z. Tan, S. Dong, *CCS Chem.* 2020, **3**, 1690.
25 G. Zeng, Y. Dong, J. Luo, Y. Zhou, C. Li, K. Li, X. Li, J. Li, *ACS Nano* 2024, **18**, 9451.
26 B. Zhan, L. Zhang, Y. Deng, L. Yan, *Green Chem.* 2023, **25**, 10061.
27 B. Zhang, G. Zhang, C. Ma, G. Zhang, *Adv. Funct. Mater.* 2025, **35**, 2415944.
28 Q. Zhu, R. Li, Y. Yan, Y. Huang, H. Su, Y. Dong, X. Pan, W. Sun, X. Wang, H. Meng, R. Wang, H. Ouyang, Y. Hong, *Adv. Funct. Mater.* 2024, **34**, 2402734.
29 Z. Chen, C. Song, X. Lian, B. Xu, Y. Wang, *Adv. Funct. Mater.* 2024, **34**, 2400829.
30 S. Luo, N. Wang, Y. Pan, B. Zheng, F. Li, S. Dong, *Small* 2024, **20**, 2310839.
31 Z.-H. Wang, B.-W. Liu, F.-R. Zeng, X.-C. Lin, J.-Y. Zhang, X.-L. Wang, Y.-Z. Wang, H.-B. Zhao, *Sci. Adv.* 2022, **8**, eadd8527.
32 J. Zhang, W. Wang, Y. Zhang, Q. Wei, F. Han, S. Dong, D. Liu, S. Zhang, *Nat. Commun.* 2022, **13**, 5214.
33 J. Xue, Z. Liang, Q. Yan, S. Zhang, H. Kang, *Nano Lett.* 2024, **24**, 3290.
34 Y. Fu, S. Chen, X. Chen, H. Zheng, X. Yan, Z. Liu, M. Wang, L. Liu, *Adv. Funct. Mater.* 2024, **34**, 2314561.
35 Z. Wu, J. Dong, H. Guo, R. Shang, X. Qin, Y. Xia, X. Li, X. Zhao, C. Ji, Q. Zhang, *Small* 2024, **20**, 2401815.
36 X. Wu, M. Li, H. Li, H. Gao, Z. Wang, Z. Wang, *Small* 2024, **20**, 2311131.
37 F. Van Lijsebetten, T. Maiheu, J. M. Winne, F. E. Du Prez, *Adv. Mater.* 2023, **35**, 2300802.
38 P. Sun, Y. Li, B. Qin, J.-F. Xu, X. Zhang, *ACS Mater. Lett.* 2021, **3**, 1003.
39 W. Guan, W. Jiang, X. Deng, W. Tao, J. Tang, Y. Li, J. Peng, C. Chen, K. Liu, Y. Fang, *Angew. Chem. Int. Ed.* 2023, **62**, e202303506.
40 H. Wang, X. Shi, Y. Xie, S. Gao, Y. Dai, C. Lai, D. Zhang, C. Wang, Z. Guo, F. Chu, *Cell Rep. Phys. Sci.* 2023, **4**, 101374.
41 X. Wu, H. Li, P. Chen, J. Zhang, M. Li, S. Zhao, Z. Wang, Z. Wang, *J. Mater. Chem. A* 2023, **11**, 6286.
42 S.-W. Chen, P. Lu, Z.-Y. Zhao, C. Deng, Y.-Z. Wang, *Chem. Eng. J.* 2022, **446**, 137304.
43 P. Sun, S. Mei, J. Xu, X. Zhang, *Adv. Sci.* 2022, **9**, 2203182.
44 Y. Yao, Z. Xu, B. Liu, M. Xiao, J. Yang, W. Liu, *Adv. Funct. Mater.* 2021, **31**, 2006944.
45 S. Wu, C. Cai, F. Li, Z. Tan, S. Dong, *Angew. Chem. Int. Ed.* 2020, **59**, 11871.